Journal of Colloid and Interface Science 469 (2016) 296–309

Contents lists available at ScienceDirect

Journal of Colloid and Interface Science

journal homepage: www.elsevier.com/locate/jcis

Metalloporphyrins immobilized in Fe_3O_4@SiO_2 mesoporous submicrospheres: Reusable biomimetic catalysts for hydrocarbon oxidation

Isaltino A. Barbosa [a], Paulo C. de Sousa Filho [a], Douglas L. da Silva [a], Fabrício B. Zanardi [a], Lucas D. Zanatta [a], Adilson J.A. de Oliveira [b], Osvaldo A. Serra [a], Yassuko Iamamoto [a,*]

[a] Bioinorganic Chemistry and Rare Earth Laboratories, Department of Chemistry, Faculdade de Filosofia, Ciências e Letras de Ribeirão Preto, University of São Paulo, Av. Bandeirantes, 3900, 14040-901 Ribeirão Preto, SP, Brazil
[b] Department of Physics, Federal University of São Carlos, Av. Trabalhador São-Carlense, 400 – Pq. Arnold Schimidt, 13566-590 São Carlos, SP, Brazil

HIGHLIGHTS

- Recyclable biomimetic catalysts.
- Metalloporphyrins inside magnetic core@shell mesoporous silica.
- Selective hydrocarbon hydroxylation and excellent epoxidation performance.

GRAPHICAL ABSTRACT

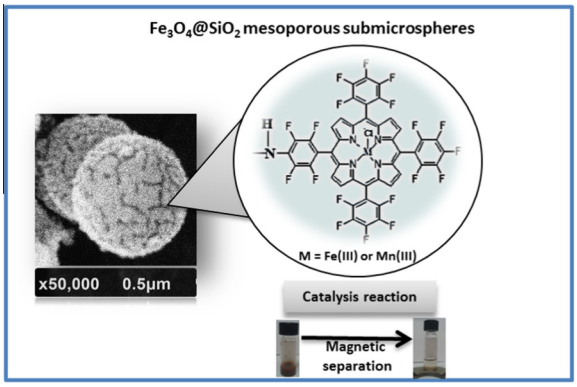

ARTICLE INFO

Article history:
Received 16 December 2015
Revised 23 January 2016
Accepted 26 January 2016
Available online 27 January 2016

Keywords:
Mesoporous structures
Core@shell structures
Magnetite particles
Porphyrins
Biomimetic catalysis

ABSTRACT

We successfully immobilized metalloporphyrins (MeP) in mesoporous silica coating magnetite spheres. In this sense, we prepared two different classes of core@shell supports, which comprise aligned (Fe_3O_4-AM-MeP, MeP = FeP or MnP) and non-aligned (Fe_3O_4-NM-MeP, MeP = FeP or MnP) mesoporous magnetic structures. X-ray diffractometry and energy dispersive X-ray spectroscopy confirmed the mesoporous nature of the silica shell of the materials. Magnetization measurements, scanning and transmission electron microscopies (SEM/TEM), electrophoretic mobility (ζ-potential), and infrared spectroscopy (FTIR) also confirm the composition and structure of the materials. The catalysts maintained their catalytic activity during nine reaction cycles toward hydrocarbon oxidation processes without detectable catalyst leaching. The catalysis results revealed a biomimetic pattern of cytochrome P450-type enzymes, thus confirming that the prepared materials are can effectively mimic the activity of such groups.

1. Introduction

Synthetic metalloporphyrins (MePs) have been used as biomimetic catalysts of Cytochrome P450 enzymes and raise great

* Corresponding author.
E-mail address: iamamoto@usp.br (Y. Iamamoto).

http://dx.doi.org/10.1016/j.jcis.2016.01.059
0021-9797/

interest [1–6], particularly in the case of Fe(III) and Mn(III) complexes [7]. Several authors have extensively studied MeP-catalyzed alkene epoxidation and alkane hydroxylation in homogeneous medium [4,8]. Although these studies revealed highly efficient systems [9], researchers pointed that homogeneous catalysts possess some critical drawbacks. For example, they can undergo self-destruction during the reaction, not to mention the difficult catalyst recovery at the end of the reaction for further reuse [10,11].

A common strategy to overcome the aforementioned limitations was the development of heterogeneous catalysts, which comprise MePs attached to a variety of solid supports. Several research groups have worked with various types of supports, namely clays [12], mesoporous silica [13–15], and zeolites, among others [16]. In this context, magnetic core@shell structures have currently drawn an increasing attention as supports for the achievement of heterogeneous catalysts and also for other applications. For instance, researchers usually synthesize the silica-coated Fe_3O_4 particles (Scheme 1, **I** and **II**) and the MePs are immobilized by electrostatic interaction [17,18] or by means of organofunctionalization, commonly with the use of 3-aminopropyltriethoxysilane (APTES) [19].

Currently, various types of novel core@shell magnetic mesoporous silica composites (Scheme 1, **I**–**IV** and **I**–**V**) have gained much attention for applications in catalysis [20,21]. These materials must display several adequate characteristics, mainly a large surface area that can undergo chemical modification to enable the immobilization of countless types of complexes [20–22], usually inside the silica mesopores. Accordingly, these systems provide a convenient method to remove the catalyst from the reaction medium, since it is only necessary to apply an appropriate magnetic field [20–23].

In this sense, core@shell magnetic mesoporous silica composites are interesting supports for MePs since, according to Mansuy [4], progress is still required to further improve these metalloporphyrin-based systems, mainly in the sense of the amelioration of the selectivity of substrate recognition by the catalyst or the support of the catalyst.

In the last decade metalloporphyrins have been highlighted as responsible for oxidation reactions using oxygen donors as PhIO and molecular oxygen, among others [16,24,25]. In this context, Huang et al. [24] reported iron meso-*tetrakis*(pentafluorophenyl)-porphyrin immobilized on zinc oxide as catalyst for cyclohexane oxidation in aerobic condition. This study therefore reinforces that preliminary studies are still necessary to evaluate the influence of different supports in catalysis performance of the MePs aiming at possible industrial applications of these ecofriendly catalyst systems [24,25].

Recently [19], we described the preparation of ordered mesoporous materials loaded with magnetic spheres inside the porous cages, which consist in Fe_3O_4 particles embedded into micrometric-sized silica structures. In such systems, manganese metalloporphyrins were immobilized via the post-synthesis methodology and the effect of pore expansion was investigated with regard to the catalytic properties of MePs in hydrocarbon oxidation. However, such report and other related papers do not discuss catalytic properties considering the different contributions of porphyrin groups inside pores and in the outer surface of the silica particles. Moreover, descriptions concerning the effects of pore ordering in the catalytic hydrocarbon oxidation by MePs and clear comparisons among covalently bound and electrostatically immobilized porphyrins in such systems are rather scarce in the literature. Therefore, in this paper we describe the synthesis of the new mesoporous magnetic catalysts and the support influence on the biomimetic behavior of metalloporphyrins as catalysts in the oxidation of hydrocarbons. Different Fe_3O_4@SiO_2 sub-micrometric structures were prepared, where isolated Fe_3O_4 particles were individually coated by silica layers (Scheme 1). This, in turn, enables the obtainment of catalysts that are readily dispersible both in water and organic solvents, presenting an improved colloidal stability, as confirmed by ζ potential measurements Hence, cyclohexane hydroxylation and (*Z*)-cyclooctene epoxidation by iodosylbenzene (PhIO) were evaluated, as well as the potential reuse of the synthesized systems. Iron(III) or manganese(III) complexes of 5,10,15,20-*tetrakis*(pentafluorophenyl)porphyrin (FeP and MnP, respectively) were covalently bonded in mesoporous silica layers coating magnetite spheres by means of APTES using the co-condensation method. Complementarily, cationic manganese (III) complexes of 5,10,15,20-*tetrakis*(4-*N*-methylpyridyl) porphyrin (MnTMPyP) were immobilized in mesoporous silica layers by electrostatic interaction for further comparison. Magnetic catalysts involving distinct silica arrays were prepared, namely (i) aligned mesoporous silica (Fe_3O_4-AM-MeP, Scheme 1, **IV**), (ii) non-aligned mesoporous silica (Fe_3O_4-NM-MeP, Scheme 1, **V**) and (iii) a control consisting in MePs immobilization only at the silica

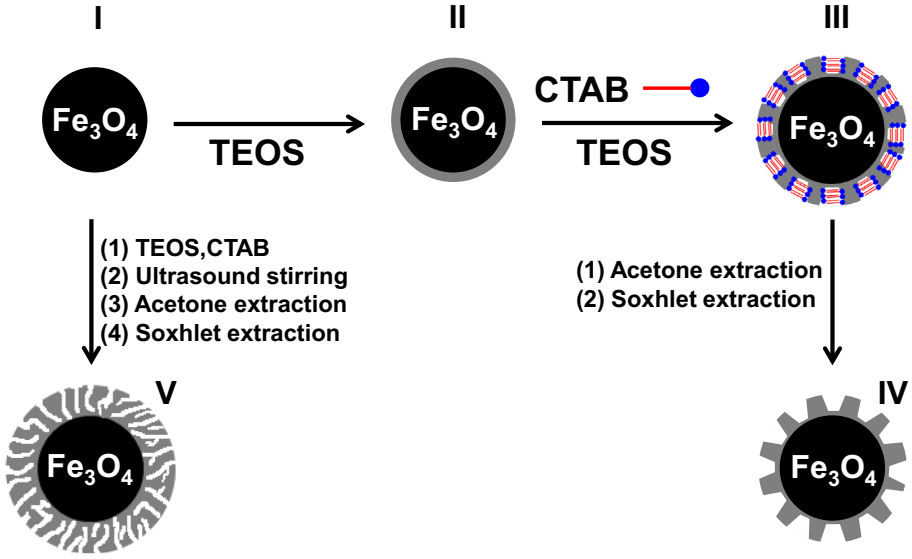

Scheme 1. Synthesis of the core@shell magnetic materials consisting in magnetite particles coated by aligned and non-aligned mesoporous silica.

surface (Fe_3O_4-SM-MeP, Scheme 1, **III**) in order to assess better the influence of the mesopores in the catalytic results.

2. Experimental

2.1. Chemicals

Iron(III) chloride hexahydrate ($FeCl_3{\cdot}6H_2O$, 97%) was purchased from Sigma and employed to synthesize the Fe_3O_4 particles. *N*,*N*-dimethylformamide (DMF, Acros) previously dried, distilled at reduced pressure and kept over 3 Å molecular sieves; 1,2-dichloroethane (DCE, Acros, 99.5%); dichloromethane (DCM, Acros, 99.5%); methanol (MeOH, Sigma); ethanol (EtOH, Aldrich 99.8%); and bromobenzene (99.5%, Aldrich) were also used. Hydrochloric acid (HCl, 37%), sodium acetate (NaAc, 99%) and ethylene glycol (EG, 99%) were acquired from Merck. The [$Fe^{(III)}$(TPFP)Cl] (FeP) metalloporphyrin, where TFPP denotes the 5,10,15,20-*tetrakis*(pentafluorophenyl)porphyrinato ligand, was acquired from Aldrich (95%). The manganese(III) complex of 5,10,15,20-*tetrakis*(pentafluorophenyl)porphyrin was synthesized from the free base porphyrin, H_2TPFFP (95%, Aldrich), following a previously described methodology [26] (Supporting Information). The synthesis of meso-tetra(*N*-methyl-4-pyridyl)porphyrinmanganese(III) chloride ([MnTMPyP]Cl_5) was performed through the reaction of H_2[TMPyP]Cl_4 with $MnCl_2{\cdot}4H_2O$ in deionized water under reflux (Supporting Information). Iodosylbenzene (PhIO) was prepared by hydrolysis of iodosylbenzene diacetate (Aldrich) by following the method of Sharefkin and Saltzman [27], PhIO purity was 90.9%, as checked by iodometric titration. The substrates used in the catalytic assays were (*Z*)-cyclooctene (Acros, 95%) and cyclohexane (Aldrich, 99.5%), which were purified by column liquid chromatography on basic alumina prior to their use. Their purities were checked by gas chromatography analysis. To obtain the inorganic framework, tetraethoxysilane (TEOS, Acros, 98%) was used as the silica source. The silylating agent was (3-aminopropyl) triethoxysilane (APTES, Aldrich, 99%), the surfactants were cetyltrimethylammonium bromide (CTAB, Acros, 98%) and poly (ethylene glycol)-block-poly(propylene glycol)-block-poly (ethylene glycol) (Pluronic P123, Sigma).

2.2. Preparation of the magnetite particles (Fe_3O_4)

The Fe_3O_4 particles were obtained according to a microwave solvothermal approach described by Zhang et al. [28] Firstly, P123 (0.80 g) was dissolved in ethylene glycol (40.0 mL) followed by addition of $FeCl_3{\cdot}6H_2O$ (1.0 g) and NaAc (3.6 g) to the mixture under vigorous stirring, until a stable suspension was achieved. The suspension was then transferred to a Teflon digestion vessel (80 mL capacity) and deaerated with an argon flux for 10 min. The mixture was then heated under microwave irradiation in a Milestone StartSynth system (1200 W of maximum power, ν = 2.45 GHz); with a software-set power in order to attain a heating step of 10 min from room temperature to 210 °C and a plateau at 210 °C for 30 min. The resulting magnetite particles were collected and removed from the solution by applying an external magnetic field. The particles were washed with water and ethanol six times followed by drying under vacuum over silica for 24 h.

2.3. Coating of the magnetite particles with silica

In order to coat the magnetite nanoparticles with a first non-ordered silica layer (Scheme 1, **I** and **II**) [22], Fe_3O_4 particles (0.1 g, prepared as described above) were treated with 0.10 mol L^{-1} HCl (50 mL) by ultrasonication for 10 min. Then, the magnetite particles were separated and washed with deionized water, followed by homogeneous dispersion in a mixture of ethanol (80 mL), deionized water (20 mL), and concentrated ammonia (1 mL, 28% m/m) for 30 min. Following, TEOS (70 μL) was added dropwise under vigorous stirring. At the end of the addition, the mixture was kept under stirring at room temperature for 6 h. The submicrospheres (Fe_3O_4@*n*SiO_2) were separated by magnetic decantation and washed with ethanol and water six times.

2.4. Synthesis of the precursor monomer

Before the growth of the final silica layer and porphyrin immobilization, a precursor monomer, which consists in an APTES group covalently bound to the macrocycle after an aromatic nucleophilic substitution reaction, was prepared (Scheme 2). For this, we applied the methodology described by Bolzon et al. [13] in which MeP (5.3 μmol) was dissolved in previously dried and deaerated DMF (5 mL) for 2 h under argon atmosphere, followed by the addition of APTES (20 μmol) at a MeP/APTES molar ratio of ~1:4. The system was kept at 80 °C for 48 h, under argon atmosphere.

2.5. Metalloporphyrins bonded in the aligned mesoporous silica layer through 3-aminopropyltriethoxysilane (APTES)

The procedure of the preparation of catalysts containing an aligned mesoporous silica layer, which are denoted as Fe_3O_4-AM-MeP, involves an adaptation of the methodology described by Deng et al. [22]. The as-prepared Fe_3O_4@*n*SiO_2 particles (110 mg, Section 2.3) were re-dispersed in a solution containing cetyltrimethylammonium bromide (0.30 g, CTAB), deionized water (80 mL), absolute ethanol (70 mL), and concentrated aqueous NH_3 (1.2 mL, 28%), which were kept under magnetic stirring for 30 min to obtain a homogenous dispersion. Then, 1.92 mmol (860 μL) of TEOS were added dropwise under vigorous stirring, followed by addition of the previously synthesized precursor monomer in DMF (Section 2.4). The suspension was kept under continuous stirring for 6 h. The material was separated with a permanent magnet, washed with deionized water and ethanol three times, and dried under vacuum. With the purpose of to remove the template CTAB and others unbound reagents, the purified catalyst was re-dispersed in acetone (60 mL) and refluxed for 48 h, this procedure was repeated three times. Finally the catalyst was washed with ethanol in a Soxhlet extractor for 120 h, and the catalyst was washed with deionized water, and dried under vacuum for 24 h, to afford the Fe_3O_4-AM-MeP compound.

In order to compare the effect of metalloporphyrin immobilization inside and outside the mesoporous silica shell channels on the oxidation process, the Fe_3O_4-SM-MeP control material was also obtained by a post-synthesis treatment. In this case, the precursor monomer was immobilized on the surface of a Fe_3O_4-AM support before the CTAB extraction (Scheme 1, **III**). In other words, the preparation of the Fe_3O_4-AM-MeP catalyst, involves a co-condensation synthesis procedure, where the precursor monomer (APTES-MeP; MeP = FeP or MnP, Scheme 2) was added during the formation of the mesoporous silica shell channels. In the obtainment of the Fe_3O_4-SM-MeP material, the APTES-MeP moieties were immobilized outside the mesoporous silica shell channels. For this, in a first step, supports were obtained according to the methodologies above described without the CTAB extraction steps and without the addition of the precursor monomer. The solids (200 mg) were thereafter dried in vacuum and, subsequently, added to 10 mL of dried and deaerated DMF containing the precursor monomer (MeP = 5.3 μmol and APTES = 20 μmol), prepared as described; the reactions were kept for 24 h under argon atmosphere. After, the materials were decanted with a magnet and the same protocol described for the surfactant removal was applied, thus yielding the catalyst containing the porphyrin groups

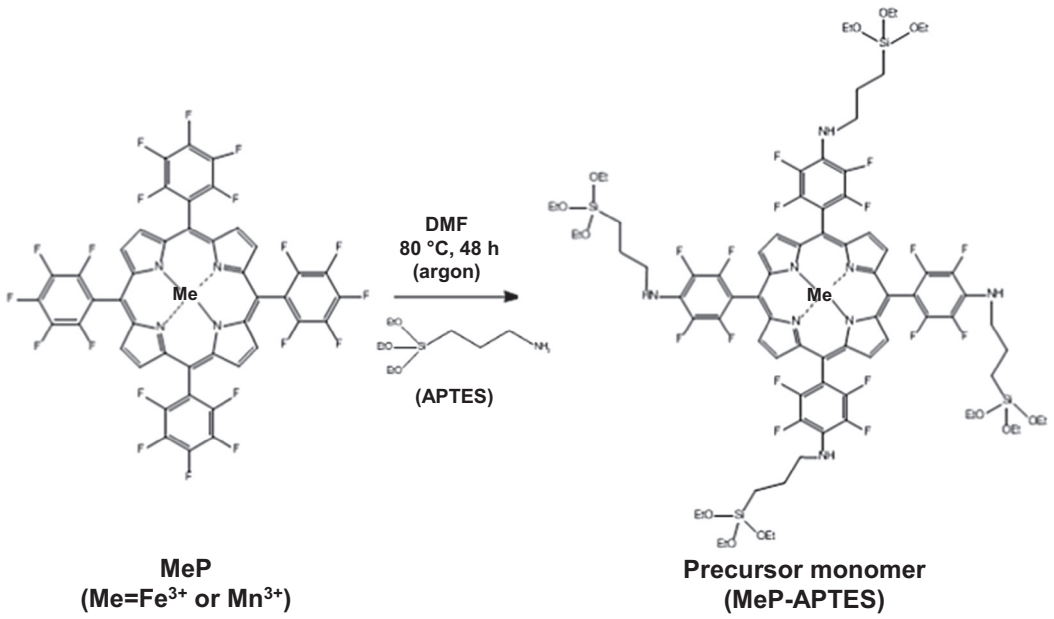

Scheme 2. Representation of the precursor monomer synthesis.

only at the surface (herein denoted Fe_3O_4-SM-MeP control material).

2.6. Metalloporphyrins bonded in the non-aligned mesoporous silica layer through 3-aminopropyltriethoxysilane (APTES)

The supports were synthesized according to the methodology described by Liu et al. [23]. To this end, 0.10 g of the as-prepared Fe_3O_4 spheres were homogeneously dispersed in a mixture containing ethanol (80 mL), deionized water (10 mL), concentrated NH_3 (4 mL), and CTAB (0.3 g) by ultrasonication (frequency = 40 kHz, power = 150 W) for 10 min. Subsequently, TEOS (0.25 mL) in ethanol (24 mL) and the precursor monomer (Scheme 2, Section 2.4) in DMF were added into the system, which was kept under ultrasonication for 20 min. The material was then separated with a permanent magnet, washed with deionized water and ethanol three times, and dried under vacuum. Finally, the purified catalyst was re-dispersed in acetone (60 mL) and refluxed for 48 h to remove the template CTAB and unbound reagents; this procedure was repeated three times. Subsequently, the catalyst was washed with ethanol in a Soxhlet extractor for 120 h, and dried under vacuum for 24 h, to yield the non-aligned Fe_3O_4-NM-MeP.

2.7. Cationic metalloporphyrin bonded to the mesoporous silica layer through electrostatic interactions

Catalysts were obtained according to methodologies describe above in Sections 2.5 and 2.6, without precursor monomer in the synthesis procedure. Subsequently, 300 mg of the Fe_3O_4-NM (or Fe_3O_4-AM) were dispersed in 40 mL of methanol and 5.3 μmol of $[MnTMPyP]Cl_5$ were added to the reaction medium. This suspension was left to rest for 24 h, and the supernatant was removed. The Fe_3O_4-NM-(MnTMPyP) and Fe_3O_4-AM-(MnTMPyP) materials were extensively washed with deionized water and methanol, and after dried at 60 °C.

2.8. Determination of the MeP loading onto the magnetic silica mesoporous material

The loading porphyrin contents were quantified by UV–Vis spectrometry on a HP 8453 spectrophotometer. For this, the extraction residues after the washing procedures (reflux and Soxhlet or direct rinsing) containing the non-immobilized MePs were collected, concentrated in a rotatory evaporator and diluted to a known volume with ethanol. The amount of MeP was determined by spectrophotometry and the loaded amount was calculated from the difference between the initial amounts of MePs (shown on the Sections 2.4 and 2.7) and the amounts of non-immobilized MeP.

2.9. Characterization and apparatus

The solids were characterized by powder X-ray diffractometry (XRD) in a Siemens D5005 diffractometer using Cu Kα radiation (1.541 Å) selected by a graphite monochromator. The morphology of prepared compounds was evaluated by scanning (SEM) and transmission (TEM) electron microscopy on a Zeiss EVO 50 and on a Tecnai G2F20 microscope coupled to energy dispersive X-ray spectroscopy (EDX) apparatus, respectively. Thermal analysis data (thermogravimetry, TGA, derivative thermogravimetry, DTG) were acquired on a TA Instruments SDT 2960 thermobalance in synthetic air atmosphere (100 mL min^{-1}). The change in ζ-potential of the materials as a function of the pH was measured by dynamic light scattering using a Malvern Instrument Zeta Sizer Nano Series ZS90. For this purpose, the solid samples were dispersed in water (1 mg mL^{-1}) containing sodium chloride (0.010 g) to attain a constant ionic strength. The pH values were regulated between 3 and 12 by addition of 1 mol L^{-1} HCl or NaOH solution to the samples, which were then submitted to the electrophoretic mobility measurements for determination of ζ-potentials. The infrared spectra (FTIR) were acquired on a Shimadzu IR Prestige21 spectrophotometer in KBr pellets, with a resolution of 2 cm^{-1}. Magnetization measurements were performed on an EG&G Princeton Applied Research vibrating sample magnetometer (VSM, 10 kOe). The specific surface area (SSA) of the prepared powders was calculated from N_2 adsorption/desorption data through the application of the Brunauer-Emmett-Teller method (BET). For this, the previously dried samples (at 100 °C in vacuum over silica, in an Abderhalden system) were submitted to adsorption of high purity N_2 (g) in a liquid N_2 bath (77 K) on a Quantachrome Autosorb 1 equipment. Gas chromatography (GC) was conducted on a HP 6890 chromatograph equipped with a flame ionization detector, using nitrogen as flow gas, and

compressed air and hydrogen helped to maintain the flame (300 mL min^{-1} flux for all gases). An HP-Innowax capillary column (cross-linked polyethylene glycol, 30 m length, 0.25 mm internal diameter, and 0.25 μm thick liquid film) was used to acquire the gas chromatograms.

2.10. Catalytic oxidation reactions

The oxyfunctionalization ability of the prepared compounds was analyzed by GC. In these tests, (*Z*)-cyclooctene and cyclohexane, were used as organic substrates; whereas iodosylbenzene (PhIO) was employed as the oxidizing agent. In all cases, bromobenzene was used as the internal standard.

The (*Z*)-cyclooctene epoxidation reactions were performed in 1,2-dichloroethane (DCE) or in dichloromethane/acetonitrile (DCM/ACN, 1:1, v/v), using a MeP/PhIO molar ratio of 1/100 ($2.5 \times 10^{-7}/2.5 \times 10^{-5}$ mol/mol) considering the amount of MeP loaded on the inorganic matrices (Table 1). Firstly, DCE (800 μL) or 400 μL de DCM and 400 μL of the acetonitrile were added to the flask containing the oxidant and the catalyst. Subsequently, (*Z*)-cyclooctene (200 μL) and bromobenzene (5 μL, standard) were added. The mixture was stirred at room temperature in air atmosphere. Aliquots (1 μL) of the reaction mixture were collected at the selected times and the product yield was analyzed by GC. This process was conducted until the end reaction. Further, the Fe_3O_4-AM-MeP, Fe_3O_4-NM-MeP, Fe_3O_4-SM-MeP catalysts were employed in consecutive reuse reactions. The reaction conditions were the same as those adopted for the experiments reported above. After each reaction, the reaction mixture was decanted by application of a magnetic field; the catalyst was washed with methanol (1 mL) four times, and dried at 50 °C for 30 min in air in an oven. Turnover numbers (TON), defined as mol of product per mol catalyst were calculated according to Sacco et al. [3]. Total turnovers were calculated according to the method described by Bolzon et al. [13].

Cyclohexane oxidation was also investigated by GC, also with PhIO as oxidizing agent. The FeP/PhIO/cyclohexane molar ratio of: 1/10/6000 ($3.0 \times 10^{-7}/3.0 \times 10^{-6}/1.8 \times 10^{-2}$), 1/40/6000 ($2.5 \times 10^{-7}/1.0 \times 10^{-5}/1.5 \times 10^{-3}$) and 1/50/5000 ($3.0 \times 10^{-7}/1.5 \times 10^{-5}/1.5 \times 10^{-3}$), considering the loading of the MeP on the inorganic matrices (Table 1). The reactions were performed in a flask using cyclohexane (200 μL), DCE (400 μL) or 400 μL of DCE/ACN (1/1, v/v) or DCM/ACN (1/1, v/v) in the presence of the oxidant and the catalyst. After the addition of bromobenzene (2 μL), the mixture was stirred at room temperature in air atmosphere for 24 h. Aliquots (1 μL) of the reaction mixture were collected and the product yield was analyzed by GC.

Supernatants of the catalysts washing procedures after reuse tests were also monitored by UV–Vis spectroscopy, in order to verify whether any MeP was leached form the inorganic matrices during the proposed protocols.

For further comparisons, the MePs as homogeneous catalysts in (*Z*)-cyclooctene and cyclohexane oxidation reactions by PhIO were investigated employing a procedure similar to that used in the case of heterogeneous catalysis and the catalysis yields were calculated based on the initial amount of PhIO added, the considerations made to use this method of quantification of the product of catalysis is detailed by Nunes et al. [29] and employed by various authors [8,10–14].

Table 1
Amounts of MePs immobilized in the Fe_3O_4-AM, Fe_3O_4-NM and Fe_3O_4-SM materials as determined by UV–Vis spectrometry.[a]

Entry	Catalysts	Loading (mol g^{-1})
1	Fe_3O_4-AM-FeP	8.0×10^{-6}
2	Fe_3O_4-NM-FeP	4.7×10^{-6}
3	Fe_3O_4-SM-FeP	1.8×10^{-5}
4	Fe_3O_4-AM-MnP	5.9×10^{-6}
5	Fe_3O_4-NM-MnP	5.4×10^{-6}
6	Fe_3O_4-SM-MnP	2.1×10^{-5}
7	Fe_3O_4-AM-(MnTMPyP)	3.0×10^{-5}
8	Fe_3O_4-NM-(MnTMPyP)	3.4×10^{-5}

[a] Molar absorptivity coefficients (ε): FeP in ethanol – $\varepsilon = 8.20 \times 10^4$ L mol^{-1} cm^{-1} at $\lambda = 413$ nm; MnP in dichloromethane – $\varepsilon = 9.38 \times 10^4$ L mol^{-1} cm^{-1} at $\lambda = 460$ nm; and MnTMPyP in acetonitrile – $\varepsilon = 9.30 \times 10^4$ L mol^{-1} cm^{-1} at $\lambda = 462$ nm.

3. Results and discussion

3.1. Morphological and structural characterization

The synthesized Fe_3O_4 particles present a clearly uniform spherical morphology, with diameters ranging around ~70-120 nm (Supporting Information, Fig. S3), which is consistent with the literature data [28]. Therefore, the fast nucleation rate allowed the production of Fe_3O_4 particles with diameters that are smaller than those achieved in conventional solvothermal methods (200–800 nm) [22,23,30].

The successful synthesis of Fe_3O_4 spheres and their crystallinity are evidenced by the powder X-ray diffractograms (Fig. 1(a)), which display the characteristic peaks at $2\theta = 30.2°$, 35.5°, 43.2°, 53.6°, 57.0°, 62.6°, and 71.1° related to the standard Fe_3O_4 pattern (JCPDS card No. 10-0319). An estimative of the crystallite sizes through the direct application of the Scherrer equation yields a value around ~19 nm. This is in agreement with the sizes estimated through the Williamson-Hall plot (inset of Fig. 1(a)), which results in a value of ~24 nm for the mean coherence length, thus attesting the nanostructural character of the prepared powder. In addition, the positive slope, as well as the low linear correlation, is a consequence of a high degree of strain and an inhomogeneity of crystalline domain sizes, which is related to the relatively mild conditions (low time and temperature), applied for the materials synthesis. This can also be related to the coexistence of a small amount of maghemite (γ-Fe_3O_4), which possess the same crystal structure of magnetite with Bragg peaks at slightly higher 2θ values (JCPDS 39-1346), which can lead to an additional broadening of the XRD peak besides polycrystallinity and strain.

Fig. 1(b) displays the XRD patterns of the final core@shell mesoporous catalysts. The diffractograms retain the same basic pattern of pure magnetite (Fig. 1(a)), thus attesting that the structure of the magnetic core is not affected. A halo emerged at angles below 30°, which confirmed the presence of amorphous silica layers [23]. In addition, diffraction peaks appeared between 2° and 3° (inset of Fig. 1b), which indicates the presence of silica mesopore channels in the catalysts [22,23].

The peak positions suggest that the spacing between the channels in the silica phase of the Fe_3O_4-AM-MeP solids is slightly smaller (~33 Å, from $2\theta = 2.62°$) than that associated to the Fe_3O_4-NM-MeP (~37 Å, from $2\theta = 2.38°$). This is in agreement with the observed pore diameters (calculated from adsorption/desorption measurements), as further discussed.

The obtainment of core@shell structures is illustrated by Fig. 2 (a) and (b), which depict the TEM images of the Fe_3O_4-NM-MeP and Fe_3O_4-AM-MeP catalysts. The images clearly display a dense Fe_3O_4 core coated by an amorphous silica shell, thus yielding structures of ~200–500 nm. In addition, the EDX intensity profiles confirm the coexistence of Fe and Si in the prepared structures. In the case of the Fe_3O_4-AM-FeP solid, the silica layer is estimated to have ~50 nm thick. Phase separation in the Fe_3O_4-NM-MeP catalyst is less evident since the non-aligned silica shell presents a lower thickness (15–20 nm). Nevertheless, in both cases, the variation

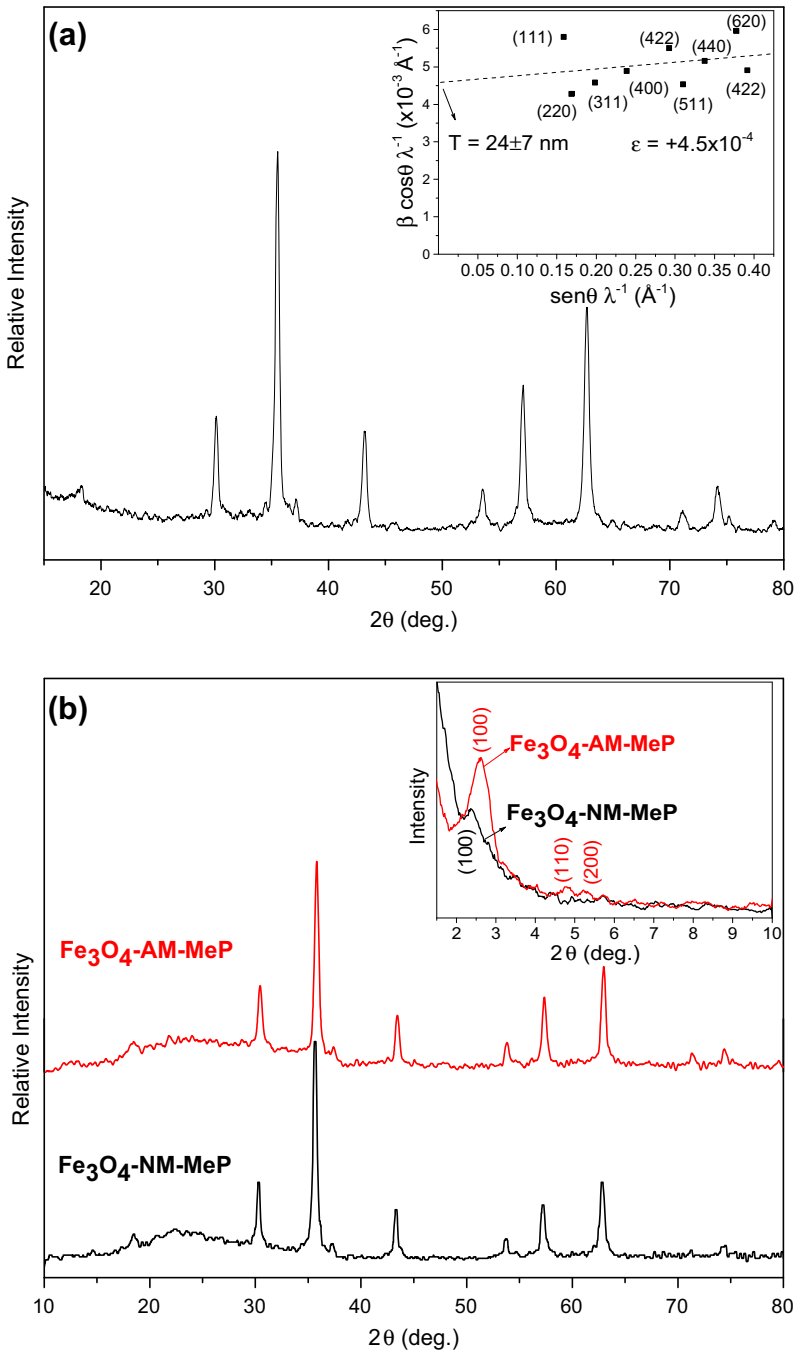

Fig. 1. Powder X-ray diffractograms of (a) submicrometric Fe_3O_4 particles (inset: Williamson–Hall plot constructed from the XRD data) and (b) Fe_3O_4-NM-MeP and Fe_3O_4-AM-FeP submicrospheres (inset: diffraction patterns at the low angle range, 1-10°).

of the Fe and Si EDX peaks along an arbitrary axis in selected particles ensures the obtainment of core@shell structures. The surface morphology of the obtained catalysts is shown by the SEM images (Fig. 2(c) and (d)), which confirm the obtainment of submicrospheres uniform in size and shape. As also observed in TEM images the Fe_3O_4-AM-MeP catalyst exhibited larger particle sizes than Fe_3O_4-NM-MeP due to its larger content of mesoporous silica shell. Additional TEM and SEM images are found in Fig. S7.

In order to evaluate the thermal behavior of the prepared powders, the TGA/DTG data were acquired and are presented in Fig. 3. Such data correspond to Fe_3O_4-AM and Fe_3O_4-NM supports, which have been prepared in the absence of the precursor monomer and, therefore, do not present organic fragments from APTES and porphyrin; the decomposition curves were measured prior to the CTAB removal procedure. For comparison, the thermal decomposition profile of a $Fe_3O_4@nSiO_2$ sample (i.e. which contains only a non-ordered silica shell grown in the absence of CTAB, Scheme 1, **I** and **II**) was also acquired. The TGA curve of this control sample (Fig. 3(c)) displays two weight loss steps. The first occurs at temperatures lower than 150 °C and are attributed to the loss of physisorbed water [31]. The second step occurs between ~200 and 300 °C and is related to the dehydration and dehydroxylation of the surface of the materials [32]. These same processes are observed in the case of Fe_3O_4-AM (Fig. 3(a)), Fe_3O_4-NM (Fig. 3(b)) samples, which, in addition, present a higher degree of weight loss between 200 and 475 °C. This is ascribed to the decomposition of

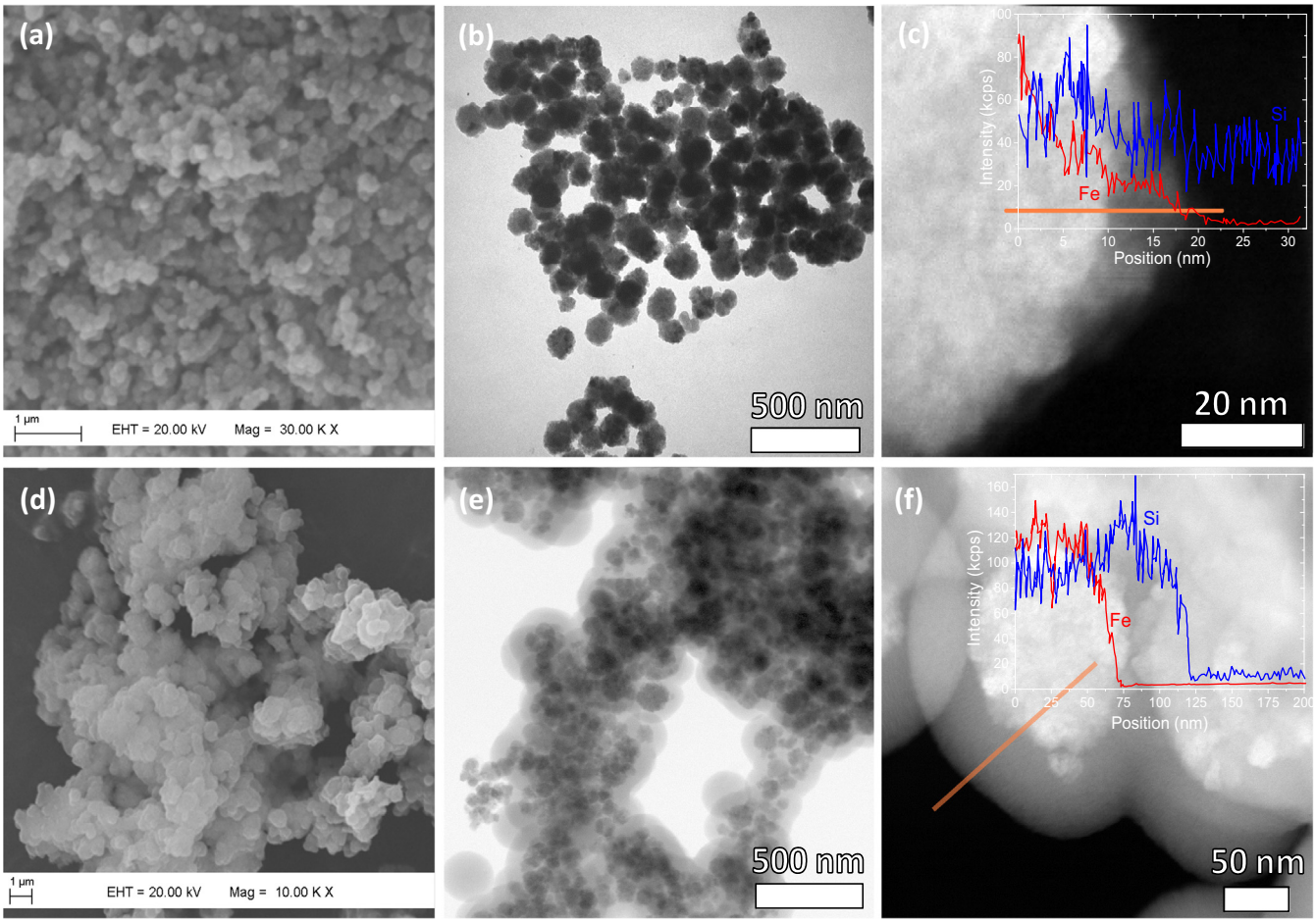

Fig. 2. SEM (a, d) and TEM (b, c, e, f) images of (a-c) Fe_3O_4-NM-MeP and (d-f) Fe_3O_4-AM-MeP samples. Insets in (c) and (f) correspond to spatially resolved Fe (red) Si (blue) EDX intensities along an arbitrary axis (orange lines). (For interpretation of the references to color in this figure legend, the reader is referred to the web version of this article.)

the surfactant groups at the same time of the loss of water through condensation of OH groups. The weight losses in the second step correspond to ~18%, 8% and 2% of the initial masses of the Fe_3O_4-AM (Fig. 3(a)), Fe_3O_4-NM (Fig. 3(b)), and Fe_3O_4@$n$$SiO_2$ (control, Fig. 3(c)) samples, respectively. This is in agreement with the larger surface area of the Fe_3O_4-AM in comparison to the other preparations, as further discussed, due to its higher amount of mesoporous silica structure. Therefore, the surfactant removal procedure can also be performed through calcinations at 450-500 °C. However, the occurrence of a partial oxidation of the magnetite core at high temperatures can be pointed by the slight increase in the sample mass observed in the thermogram of Fig. 3(c), in which after 300 °C the oxidation of Fe^{2+} result in the capture of oxygen.

In this sense, the efficiency of surfactant removal through the proposed mild conditions (reflux and Soxhlet extraction) can be accessed by the FTIR spectra of the Fe_3O_4-AM and Fe_3O_4-NM also prepared in the absence of the precursor monomer and free of CTAB (after the extraction). Such spectra are compared to a Fe_3O_4@nSiO_2@CTAB/SiO_2 sample prior to the CTAB removal procedure, which is shown in Fig. S6. The spectra (Fig. 3(d)) display bands at 3500 and 1600 cm^{-1} that correspond to the O-H symmetric/antisymmetric stretchings, and H-O-H bending vibrations of adsorbed water molecules, respectively [17,22,33]. The OH stretchings of the Si-OH groups also contributed to the band at 3500 cm^{-1}. The band around 590 cm^{-1} region is ascribed to Fe-O bonds of the magnetite [31]. The remaining bands were due to the vibrations associated with the silica matrix, namely at 1086 cm^{-1} (Si-O-Si stretchings), 955 cm^{-1} (Si-OH stretching), and 799 cm^{-1} (Si-O-Si deformation) [16]. Absorption peaks in the 2800–3000 cm^{-1} range, which corresponds to -CH_2 stretchings of the surfactant [22], were not observed in the Fe_3O_4-AM and Fe_3O_4-NM supports after the extraction procedure of the CTAB, thus attesting the efficiency of the adopted protocol (Fig. S6). The spectra of the Fe_3O_4-AM and Fe_3O_4-NM samples are essentially the same, except for the higher relative intensity of the band at ~580 cm^{-1} in the latter, which is ascribed to the lower Si/Fe ratio in this case.

The surface state of the prepared particles in aqueous medium was investigated through electrophoretic mobility measurements in order to describe the variation of the ζ-potential of the catalysts against the pH (Fig. S4). The Fe_3O_4-AM-MeP and Fe_3O_4-NM-MeP catalysts were compared to the pure magnetite particles and with the control compositions prepared without the addition of the precursor monomer (Fig. S4(a)). The pure Fe_3O_4 particles displayed positive ζ-potentials, around +24 mV at pH = 3, due to the formation of Fe–OH_2^+ species at their surface [34]. The coating effect over the magnetite surface by the silica layers is evidenced both by the reduction of the pH of isoelectric point (pH_{PI}) from $pH_{PI} \sim 4$ (Fe_3O_4) to $pH_{PI} \sim 3$ (Fe_3O_4@SiO_2), and by the diminution of the absolute value the ζ-potential at acidic conditions (Fig. S4(b)).

This occurs due to the covering of the more acidic silica surface groups (Si–OH) and due to the fact that the more basic Fe–OH groups are not exposed to the solution. On the other hand, at basic conditions, the silica-coated materials present larger absolute values of ζ ($|\zeta| \sim 40$ mV) due to the formation of negative species (Si–O^-) at a larger extent, which ensures a high colloidal stability

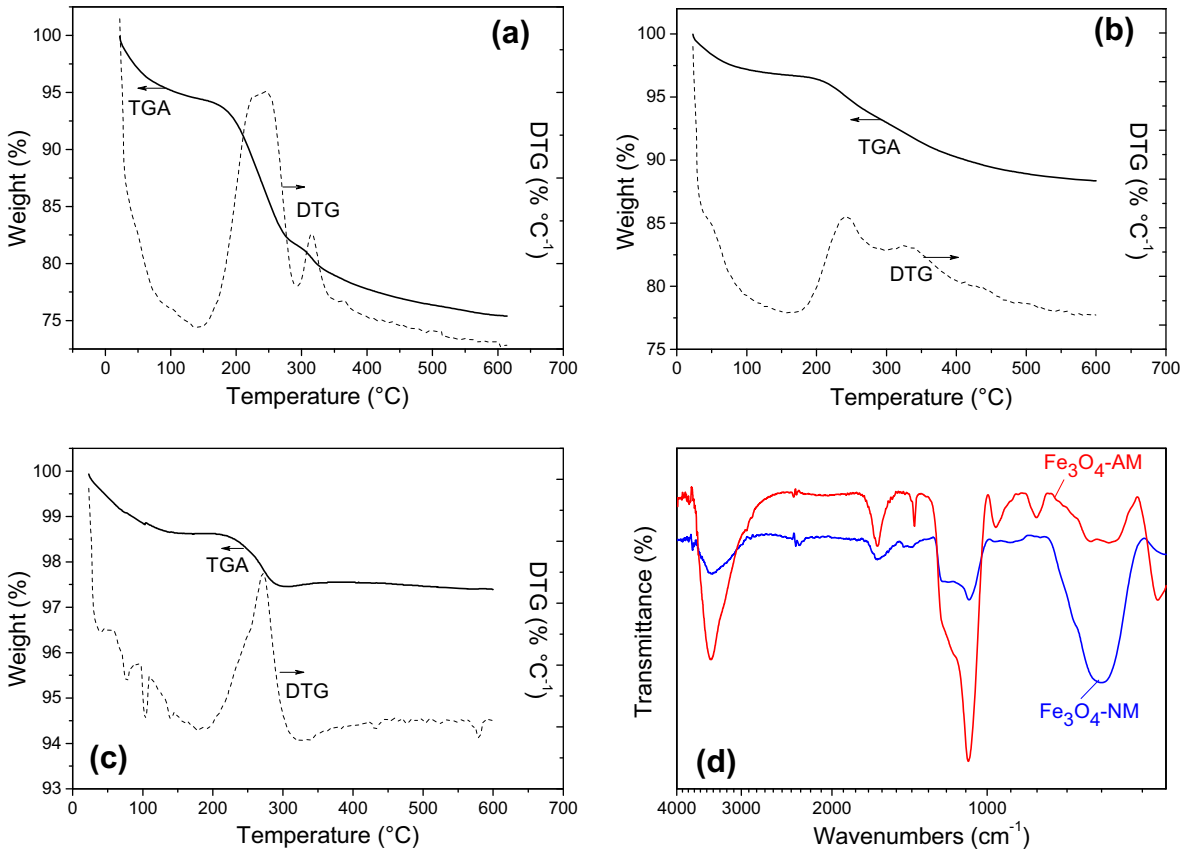

Fig. 3. TGA/DTA curves of the (a) Fe_3O_4-AM (with CTAB), (b) Fe_3O_4-NM (with CTAB), and (c) Fe_3O_4@$n$$SiO_2$ (without CTAB) samples. (d) Infrared spectra of the Fe_3O_4-AM and Fe_3O_4-NM supports after the extraction procedure.

at pH > 5 for such supports. In comparison to the control samples, the Fe_3O_4-NM-MeP and Fe_3O_4-AM-MeP catalysts (Fig. S4(a)) presented slightly shifted pH_{PI} values to, 3.2 and 4.0, respectively. This occurs due to the introduction of the APTES residues at the catalyst surfaces, which present the more basic $-NH_2$ groups [33,35,36]. The presence of free NH_2 groups is expected since the synthesis of the precursor monomer was performed in the presence of an excess of APTES (FeP/APTES = 1/4) and because the substitution in four phenyl groups of the same porphyrin is rather improbable. This leads to the presence of free NH_2 groups in the final solids which, in turn, results in higher pH_{PI} values compared to the controls. The larger shift observed for the Fe_3O_4-AM-MeP catalyst is due to its larger amount of silica phase and higher surface area, resulting in a larger amount of residual amino groups. In addition, as surface $-NH_2$ groups are more easily protonable than Si–OH, positive ζ values can be observed for the two catalysts at low pHs, which are particularly high for the Fe_3O_4-AM-MeP ($|\zeta| \sim 25$ mV). In summary, the two compositions display the characteristic behavior of APTES-functionalized supports, as well as a marked colloidal stability due to electrostatic repulsions in the 5–12 pH range.

Loadings obtained by indirect determination through UV-Vis spectrometry are shown in Table 1, indicating the presence of MeP in concentrations ranging from 10^{-5} to 10^{-6} mol per gram of support. Catalysts containing covalently bound porphyrins inside the pores (Fe_3O_4-AM-FeP, Fe_3O_4-NM-FeP, Fe_3O_4-AM-MnP, Fe_3O_4-NM-MnP, entries 1, 2, 4, and 5, Table 1) show lower loadings in comparison to the compounds containing porphyrins immobilized only at the surface (Fe_3O_4-SM-FeP and Fe_3O_4-SM-MnP, entries 3 and 6) or attached by electrostatic interaction (Fe_3O_4-AM-(MnTMPyP) and Fe_3O_4-NM-(MnTMPyP), entries 7 and 8). This occurs because covalent immobilization inside pores (Table 1, entries 1, 2, 4, and 5) involves a co-condensation synthesis process, where the precursor monomer was added during the silica mesoporous formation, and thus, in the presence of water. Therefore, due to the larger extent of hydrolysis of the ethoxy groups of the precursor monomer prior to condensation in the silica shell, a smaller amount of immobilized macrocycles is observed in these cases. On the other hand, the covalent immobilization at the surface (Table 2, entries 3 and 6) by the post-synthesis method is conducted in the absence of water, which results in higher loading yields due to the lower extent of hydrolysis. Finally, the immobilization of the cationic macrocycles through electrostatic interactions (Table 2, entries 7 and 8) is largely favored by the high degree of negative charges in the catalyst surfaces, which present negative ζ potentials in very broad pH ranges (Fig. S4). In this sense, the positive charges on the cationic (MnTMPyP) probably strongly interact with the Si-OH groups of the silica mesoporous, thus conducting to a higher degree of immobilization for (MnTMPyP) [17].

Table 2
Textural properties of the mesoporous magnetic supports.

Supports	SSA_{BET}[a] ($m^2\ g^{-1}$)	V_{BJH}[b] ($cm^3\ g^{-1}$)	dv[c] (nm)
Fe_3O_4-AM	764	0.42	2.2
Literature[d]	365	0.29	2.3
Fe_3O_4-NM	200	0.17	3.4
Literature[e]	245	0.22	3.2

[a] Multipoint BET Specific Surface area.
[b] cumulative BJH method desorption pore volume.
[c] average pore diameter.
[d] Ref. [22].
[e] Ref. [23].

Textural properties of the Fe_3O_4-AM and Fe_3O_4-NM supports (Table 2) were determined by a N_2 adsorption/desorption experiment at 77 K. The isotherms (Fig. 4) exhibit a type-IV IUPAC classification, with a steep increase in the 0.05-0.30 P/P_0 region, and a significant degree of hysteresis with completely reversible nature. This is related to the capillary condensation steps between 0.35 and 0.80 of P/P_0, which is a pattern of mesoporous materials (i.e. with pore diameters ranging from 2 to 50 nm) [37], as currently reported in the literature [22,23]. Such characteristics are further confirmed by the calculation of the specific surface areas (SSA) according to the BET equation and pore volumes and diameters through the Barrett-Joyner-Halenda (BJH) method. The Fe_3O_4-AM-MeP catalyst (Fig. 4(a)) presents a high surface area (764 $m^2\ g^{-1}$), with total pore volumes around in 0.42 $cm^3\ g^{-1}$. Pore diameter distributions present a main peak at 2.2 ± 0.5 nm and small secondary peak at 3.3 nm.

In comparison to similar compositions in the literature [22], the Fe_3O_4-AM-FeP solid shows practically the same values of mean pore diameter, due to the use of the same structure directing agent in similar conditions. On the other hand, pore volumes and SSA values are remarkably different, which is related to the use of magnetite particles of ~100 nm leading to the obtainment of smaller core@shell structures. The Fe_3O_4-NM support presents (Fig. 4(b)) a larger value of mean pore diameter (3.4 nm) in comparison to Fe_3O_4-AM support, which is a consequence of the wormlike array of channels (i.e. lack of organized structures), also in agreement with the observed XRD patterns. Moreover, this preparation results in larger SSA and pore volumes than those found in literature [22,23], which is also due to the obtainment of smaller Fe_3O_4 spheres.

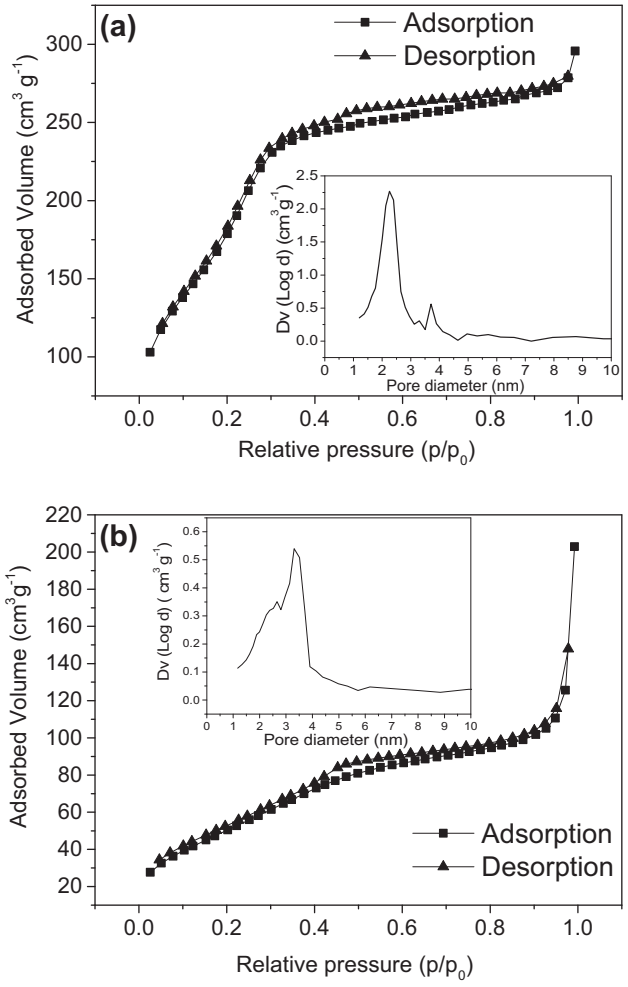

Fig. 4. N_2 adsorption/desorption isotherms of the synthesized catalysts: (a) Fe_3O_4-AM and (b) Fe_3O_4-NM (insets: mesopore size distributions).

Magnetization profiles of the Fe_3O_4 particles and the Fe_3O_4-AM-MeP, and Fe_3O_4-NM-MeP catalysts were measured through VSM (Fig. S5). The magnetization saturation (Ms) observed for Fe_3O_4, Fe_3O_4-AM-MeP, and Fe_3O_4-NM-FeP solids were found to be 37.9, 15.6 and 24.1 emu g^{-1}, respectively. The reduced Ms values observed for the core@shell solids as compared with Fe_3O_4 were due to the diamagnetic silica coating, which lowered the magnetization value by means of magnetic dipolar interactions [35,38]. The fundamental ferromagnetic behavior of magnetite samples is kept in the three cases, since all samples showed nonlinear and reversible curves, with negligible coercivity and remanence (i.e., without magnetic hysteresis), thus being characterized as soft magnetic materials. Despite the smaller Ms values obtained for the catalysts, they were still large enough for the materials to be easily separated from liquid suspensions by an action of external magnet [35].

3.2. Catalytic studies

3.2.1. Epoxidation of (Z)-cyclooctene

(*Z*)-cyclooctene is an easily oxidable substrate that usually results in the formation of cyclooctene oxide as a single oxidation product. As a consequence, cyclooctene is applied to evaluate the activity of new catalysts, in order to provide information about the accessibility of substrates and oxidants to the active sites, which is particularly important for porphyrin-based catalysts [4,13,17]. In this sense, we studied the activity of the prepared catalysts toward (*Z*)-cyclooctene epoxidation by PhIO (Table 3).

In order to better evaluate the effect of the mesoporous silica matrix on the oxidative activity of the prepared compounds, the stability of the synthesized catalysts was investigated through recycling consecutive tests conducted by carrying out a total of nine reuse cycles (Fig. 5).

The catalysts containing MePs immobilized inside silica mesopores (Fe_3O_4-AM-FeP, Fe_3O_4-NM-FeP, Fe_3O_4-AM-MnP, and Fe_3O_4-NM-MnP) yield 90%, 98%, 70% and 94% of cyclooctene oxide, respectively (Table 3, entries 2, 3, 6 and 7). The TON for these reactions ranged from 668 to 827, indicating an excellent potential for reuse. It is clearly observed that despite the lower yield in the cyclooctene epoxidation of the Fe_3O_4-AM-MnP catalyst, the calculated TON value was higher than materials containing MePs immobilized only at the surface (Fe_3O_4-SM-FeP and Fe_3O_4-SM-MnP, Table 3, entries 4 and 8; TON from 508 to 650, Fig. 5a and b). In other words, the Fe_3O_4-SM-FeP and Fe_3O_4-SM-MnP preparations present an expressive decrease in the catalytic activity during the reaction cycles, thus lowering TON values. This occurs since, in the case of surface-immobilized porphyrins, the macrocycles are more exposed to the reaction medium, being more susceptible to competitive degradation reactions when compared to groups inside the mesopores. Consequently, the pore structures of the Fe_3O_4-AM and Fe_3O_4-NM samples ensure a higher stability for these catalysts, which can also be related to their increased TON values (Table 3, entries 2, 3, 6, and 7). In addition, Fig. 5(c) also depicts a clear difference between the reusability of the materials with covalent and electrostatic immobilization. The maximum epoxidation yields of the materials containing MnTMPyP are more drastically reduced along reaction cycles in comparison to their equivalent compositions containing MnP and FeP. This is probably a consequence of the higher susceptibility of the electrostatically immobilized porphyrins to degradation processes during the recycling, thus largely reducing the reuse potential of the Fe_3O_4-AM-(MnTMPyP), and Fe_3O_4-NM-(MnTMPyP) catalysts.

Table 3
Yields of (*Z*)-cyclooctene oxidation by PhIO catalyzed by synthesized materials and comparison with MePs in homogeneous conditions.[a]

Entry	Catalyst	Cyclooctene oxide yield (%) (±5%)	Total turnover
1	FeP	100[b]	–
2	Fe_3O_4-AM-FeP	90[c]	730
3	Fe_3O_4-NM-FeP	98	802
4	Fe_3O_4-SM-FeP	97	508
5	MnP	100[b]	–
6	Fe_3O_4-AM-MnP	70	668
7	Fe_3O_4-NM-MnP	94	827
8	Fe_3O_4-SM-MnP	86	650
9	MnTMPyP[d]	83	–
10	Fe_3O_4-AM-(MnTMPyP)[d]	69	517
11	Fe_3O_4-NM-(MnTMPyP)[d]	86	515
12	Fe_3O_4-AM (control sample)[e]	20	–
13	Fe_3O_4-NM (control sample)[e]	20	–
14	PhIO, solvent and substrate	7	–
15	Fe_3O_4@*n*SiO_2@MCM-41-MnP[f]	77	421
16	Fe_3O_4@*n*SiO_2@MCM-41(E)-MnP[f]	93	590

[a] Experimental conditions: MeP/PhIO molar ratio 1:100, 200 μL (*Z*)-cyclooctene, 800 μL DCE, and 5 μL bromobenzene, stirring, room temperature, in ambient atmosphere.
[b] 10–15 min of reaction, data extracted from Ref. [13], the catalysis was performed under identical conditions to those employed for heterogeneous catalysis.
[c] Catalytic tests were performed as duplicates; yields based on the starting PhIO according to the literature [11,13,17].
[d] Experimental conditions: MeP/PhIO molar ratio 1:100, 200 μL (*Z*)-cyclooctene, 400 μL DCM, 400 μL ACN and 5 μL bromobenzene, stirring, room temperature, in ambient atmosphere, 1 h of reaction.
[e] Control catalysis (without MeP in the supports) was performed under conditions identical to those employed for heterogeneous catalysis.
[f] Results obtained of the literature [19].

Studies on the influence of the reaction time on the performance of the Fe_3O_4-NM-FeP, Fe_3O_4-AM-FeP, Fe_3O_4-SM-FeP, Fe_3O_4-NM-MnP, Fe_3O_4-AM-MnP and Fe_3O_4-SM-MnP catalysts (Fig. 6) explain how the size of the mesopores in these materials affects the oxidation process, thus, the epoxidation yields as a function of the reaction time were monitored (Fig. 6) and the time for yield stabilization ranged from 100 to 160 min. These values were high in comparison to the times for stabilization of homogeneous catalysts (10–15 min, Table 3, entries 1 and 5), which is probably due to more restricted access of the substrate to the active species in the silica matrix [39]. In the case of catalysts with electrostatic immobilization, Fe_3O_4-NM-(MnTMPyP) and Fe_3O_4-AM-(MnTMPyP), stabilization times were 90 min and 110 min, respectively, which are only slightly higher times in comparison to the 60 min required for stabilization reaction in homogeneous medium (Table 3, entry 9). The pore structure of the prepared silica matrices tend to difficult the access of substrate and oxidant molecules to the metalloporphyrin active sites, so that smaller pore diameters are more probably related to high stabilization times of epoxidation yield. This is clearly observable by comparing samples with aligned (Fe_3O_4-AM) and non-aligned (Fe_3O_4-NM) mesopores, which have mean pore diameters of 2.2 and 3.4 nm, respectively (Table 2). In the former cases, smaller pore diameters induce a lower diffusibility of substrate and oxidant toward the active sites, which culminates in increased epoxidation times in comparison to the larger pore samples (Fig. 6), as well as to other preparations in the literature [13,17]. In other words, although smaller pores of Fe_3O_4-AM samples result in large surface areas, the reduced pore sizes impose a kinetic drawback due to the lower accessibility to active sites in comparison to Fe_3O_4-NM samples.

Although in previous work our group achieved good catalytic performance in epoxidation reactions (Table 3 entries 15 and 16) using the Fe_3O_4@*n*SiO_2@MCM-41(E)-MnP composite [19], the turnover values (421 and 590, Table 3 entries 15 and 16, respectively) were lower than those obtained for the Fe_3O_4-NM-MnP and Fe_3O_4-AM-MnP magnetic core@shell catalysts here described

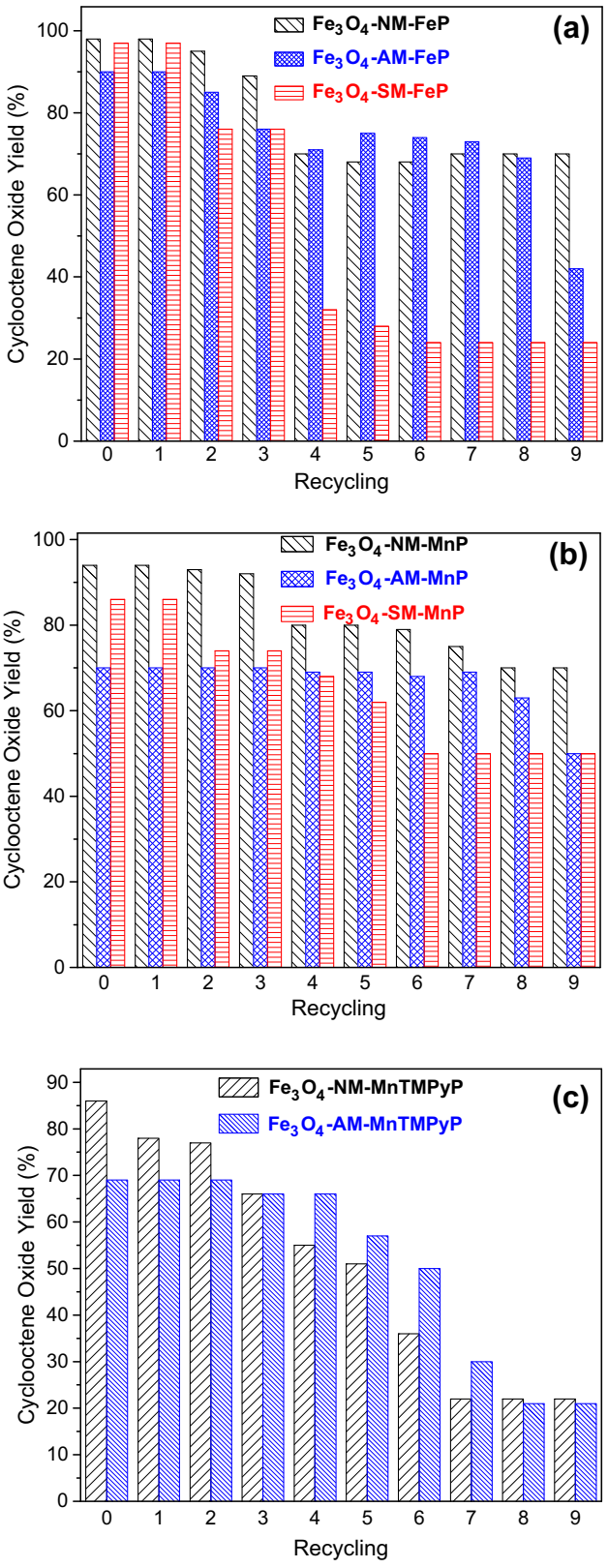

Fig. 5. Catalytic tests after nine reuse cycles in the oxidation of (*Z*)-cyclooctene by PhIO of the materials containing (a) FeP, (b) MnP, and (c) MnTMPyP porphyrins.

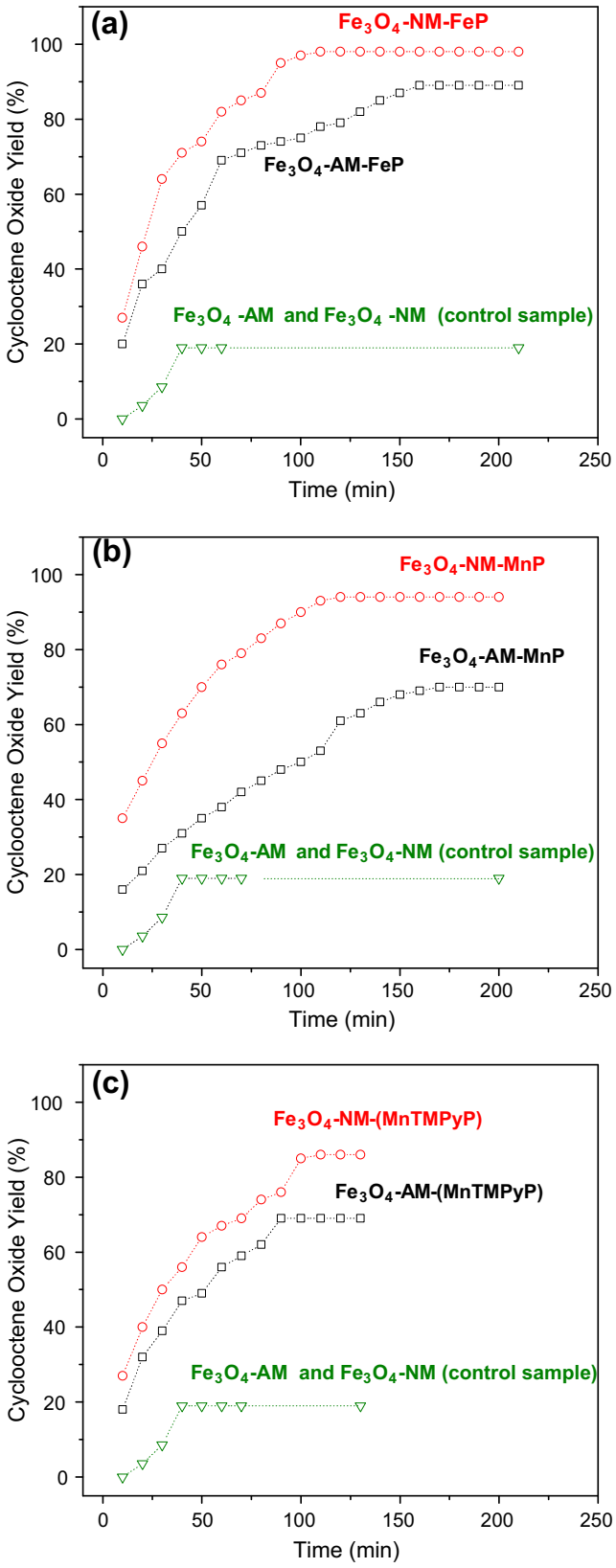

Fig. 6. The performance of the synthesized (a) Fe_3O_4-NM-FeP, Fe_3O_4-AM-FeP, (b) Fe_3O_4-NM-MnP, Fe_3O_4-AM-MnP, (c) Fe_3O_4-NM-(MnTMPyP), Fe_3O_4-AM-(MnTMPyP) catalysts during a single catalytic test of the (*Z*)-cyclooctene epoxidation.

(668 and 827, Table 3 entries 6 and 7, respectively). In addition, no organic expander molecules as mesitylene are required to achieve good catalytic performance in hydrocarbon oxidation in lower synthesis times. Therefore, the core@shell magnetic mesoporous catalysts are more eco-friendly catalysts in comparison to Fe_3O_4@*n*SiO_2@MCM-41(E)-MnP composites [19].

Dos Santos et al. [40] investigated the catalytic activity of FeP on the surface of magnetic amino-functionalized nanospheres, and they obtained 71% of cyclooctene oxide yields for reactions with *m*-cloroperoxybenzoic acid as oxidant and the molar ratio of 1:250 (catalyst/oxidant). We employed PhIO as oxidizing agent to evaluate the catalytic activity of the FeP immobilized inside the silica mesoporous, and we achieved 90% and 98% of cyclooctene oxide yields with Fe_3O_4-AM-FeP, Fe_3O_4-NM-FeP catalysts (Table 3, entries, 2 and 3, respectively). The high epoxidation efficiency of the prepared catalysts indicated a typical biomimetic pattern involving firstly a reaction of $Fe^{III}P$ with PhIO in the active site, followed by the formation of the $Fe^{IV}(O)P^{\cdot+}$ or $Fe^{V}(O)P$ intermediates in the process [2].

In addition, Bolzon et al. [13] investigated the catalytic activity of FeP and MnP immobilized into hexagonal mesoporous silica in the oxidation of (*Z*)-cyclooctene using basically the same condition herein described (i.e. a catalyst/oxidant/substrate molar ratio of 1:100:6000 and DCE as the solvent). They obtained 100% and 89% of cyclooctene oxide yield with large-pore and small-pore materials, respectively. We achieved similar results of cyclooctene oxide yields with Fe_3O_4-AM-FeP and Fe_3O_4-NM-FeP (Table 3, entry 2 and 3, respectively). However, our results for the Fe_3O_4-AM-MnP and Fe_3O_4-NM-MnP materials (70% and 94%, respectively; Table 3, entries 6 and 7), were lower than those obtained by Bolzon et al., even though the turnover data obtained in the present case (Table 3, entries 6 and 7) are more elevated than the former reported. For further comparison, Ucoski et al. [17] supported cationic metalloporphyrins (MnTMPyP) on silica-coated Fe_3O_4 nanoparticles and obtained 84% of cyclooctene oxide yield (1:50:5000 catalyst/oxidant/cyclooctene molar ratios) in 60 min of reaction. We achieved a similar result (86% of cyclooctene oxide yield) with the Fe_3O_4-NM-(MnTMPyP) catalyst, after 110 min of reaction (Table 3, entry 11, Fig. 5c).

The results of control catalysis (in the absence of MePs) revealed maximum product yields of 20% (Fig. 5), which can be probably explained by free-radical self-oxidation mechanism in the presence of dioxygen, PhIO, support and solvent [17,12].

3.2.2. Oxidation of cyclohexane

We also investigated the catalysts performance in the hydroxylation of cyclohexane. Although being a less reactive substrate than (*Z*)-cyclooctene, cyclohexane is a highly interesting substrate in selectivity studies as P450 biomimetic catalysts because it can generate cyclohexanol and/or cyclohexanone as oxidation products. In metalloporphyrin-catalyzed cyclohexane oxidation, the oxidant (in the present case, PhIO) transfers an oxygen atom with two oxidizing equivalents to form a high-valence metal intermediate ($Me^{IV}(O)P^{\cdot+}$), which abstracts a hydrogen atom of the cyclohexane molecule. This results in the formation of the $Me^{IV}(OH)P^{+}$ species and a cyclohexyl radical (C_6H_{11}), which are kept close by the formation of a solvent cage (Fig. 7). If this solvent cage is sufficiently long-lived, a transfer of a hydroxyl group from $Me^{IV}(OH)P^{+}$ to the cyclohexyl radical takes place, thus selectively producing cyclohexanol in a biomimetic process usually termed as oxygen rebound [41]. However, if a short-lived solvent cage is involved, the transfer of a hydroxyl group is not favored. In this case, the radicals may escape from the cage and react directly with the oxidant generating cyclohexanone via a non-biomimetic radicalar mechanism and leading to the loss of selectivity (Fig. 7).

In this sense, our results show that cyclohexane oxidation with $Fe^{III}P$ is selective (Table 4, entries 9 and 10) compared with the equivalent $Mn^{III}P$ (Table 4, entries 1 and 2). The loss of selectivity for $Mn^{III}P$ system, can be due to a larger cage escape [11,13]. In

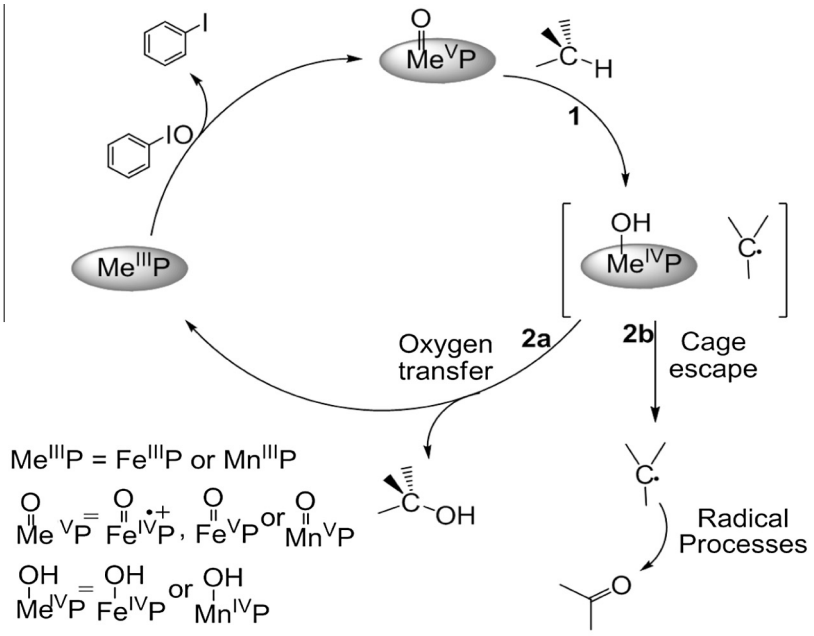

Fig. 7. Mechanism of the MeP-catalyzed oxidation of alkanes by PhIO [13].

Table 4
Cyclohexane oxidation by PhIO catalyzed by FeP and MnP in homogeneous and heterogeneous catalysts, after 24 h of reaction.

Entry	Catalyst	Solvent	%C_{ol} (±7%)	%C_{one} (±2%)	C_{ol}/C_{one}[c]
1	MnP	DCE	34[a]	16	2.1
2	MnP	DCE:ACN	40 (30)[b]	24 (13)	1.6 (2.3)
3	Fe_3O_4-AM-MnP	DCE	14	–	14
4	Fe_3O_4-AM-MnP	DCE:ACN (1:1)	20 (17)	7.0 (3.0)	2.8 (5.6)
5	Fe_3O_4-NM-MnP	DCE	9.5	–	9.5
6	Fe_3O_4-NM-MnP	DCE:ACN (1:1)	30 (36)	9.0 (9.0)	3.3 (4.0)
7	Fe_3O_4-SM-MnP	DCE	18	9.0	2.0
8	Fe_3O_4-SM-MnP	DCE:ACN (1:1)	20 (20)	12 (10)	1.6 (2.0)
9	FeP[b]	DCE	39	4.0	9.7
10	FeP[b]	DCE:ACN (1:1)	41 (46)	6.0 (5.0)	6.8 (9.2)
11	Fe_3O_4-NM-FeP	DCE	11	–	11
12	Fe_3O_4-NM-FeP	DCE:ACN (1:1)	21 (29)	1.0 (6.0)	21 (4.8)
13	Fe_3O_4-AM-FeP	DCE	10	–	10
14	Fe_3O_4-AM-FeP	DCE:ACN (1:1)	24 (17)	–	24 (17)
15	Fe_3O_4-SM-FeP	DCE	27	–	27
16	Fe_3O_4-SM-FeP	DCE:ACN (1:1)	35 (36)	6.0 (8.0)	5.8 (4.5)
	Catalysis controls				
17	Fe_3O_4-AM	DCE	–	–	–
18	Fe_3O_4-NM	DCE	–	–	–
19	Fe_3O_4-AM	DCE:ACN (1:1)	–	–	–
20	Fe_3O_4-NM	DCE:ACN (1:1)	–	–	–

[a] Results outside parentheses were obtained using: catalyst/oxidant/cyclohexane molar ratio = 1:10:6000 (MeP = 3.0×10^{-7} mol, PhIO = 3.0×10^{-6} mol and cyclohexane = 1.5×10^{-3} mol).
[b] Catalytic results in parentheses were obtained using catalyst/ oxidant/cyclohexane molar ratio = 1:40:6000 (MeP = 2.5×10^{-7} mol, PhIO = 1.0×10^{-5} mol, cyclohexane = 1.5×10^{-3} mol).
[c] C_{ol} = cyclohexanol and C_{one} = cyclohexanone; catalytic tests were performed as duplicates; yields based on the starting PhIO according with Refs. [6,8,10–14,17]; homogeneous catalysis was performed under conditions identical to those employed for the heterogeneous catalysis.

order to evaluate the activity of heterogeneous and homogeneous systems, different MeP/PhIO ratios, namely 1:10 and 1:40 were tested using DCE and DCE/ACN mixture as solvents (Table 4). In this way, it was observed that Fe_3O_4-AM-MnP and Fe_3O_4-NM-MnP catalysts in dichloroethane as solvent provide high selectivities toward cyclohexanol (Table 4, entries 3 and 5). This result is associated to the silica mesoporous structures in the magnetic supports, which provides local microenvironments that are more suitable for the formation of long-lived solvent cage (Fig. 7), thus resulting in higher biomimetic behavior. Besides, it is interesting to highlight that the selectivity is decreased for Fe_3O_4-SM-MnP in DCE (Table 4, entry 7), which provides results close to those observed for the homogeneous system (Table 4, entry 1).

In order to improve the PhIO solubility [13,17], DCE/ACN mixtures were also used. With Fe_3O_4-AM-MnP and Fe_3O_4-NM-MnP yields of catalytic products were increased (Table 4, entries 4 and 6), however it was observed a selectivity decrease. As ACN is a more polar and less viscous solvent ($\varepsilon = 37.5$, $\eta = 0.369$ mPa s, where ε denotes the relative permittivity and η the viscosity) than DCE ($\varepsilon = 10.4$, $\eta = 0.799$ mPa s), the presence of ACN probably favors the solvent cage collapse and the escape of the radicalar species [11,42].

Table 5
Cyclohexane oxidation by PhIO catalyzed by MnTMPyP in homogeneous and heterogeneous catalysts.

Entry	Catalyst	Ratio MnPy:PhIO:substrate	Solvent	C_{ol} (%) (±7%)	C_{one} (%) (±2%)	Ratio[b] C_{ol}/C_{one}
1	MnTMPyP	1:40:6000[c]	DCE:ACN (1:1)	9 (14)[a]	5 (10)	1.8 (1.4)
2	Fe_3O_4-AM-(MnTMPyP)	1:40:6000[c]	DCE:ACN (1:1)	18 (26)	1.0 (2.0)	18 (13)
3	Fe_3O_4-NM-(MnTMPyP)	1:40:6000[c]	DCE:ACN (1:1)	27 (40)	4.5 (7.0)	6 (5.7)
4	Fe_3O_4-AM-(MnTMPyP)	1:40:6000[c]	DCE	15 (26)	1.0 (8.0)	15 (3.0)
5	Fe_3O_4-NM-(MnTMPyP)	1:40:6000[c]	DCE	18 (36)	8.0 (9.0)	2.2 (4.0)
6	Fe_3O_4-AM-(MnTMPyP)	1:50:5000[d]	DCM:ACN (1:1)	13 (24)	6.5 (9.0)	2 (2.6)
	Catalysis control	Solvent				
7	Fe_3O_4-AM[e]	DCE:ACN (1:1)		–	–	–
8	Fe_3O_4@-NM[e]	DCE:ACN (1:1)		–	–	–

[a] Catalytic results in parentheses were obtained after 24 h of the reactions. Results outside parentheses were obtained after 1 h of the reactions.
[b] C_{ol} = cyclohexanol and C_{one} = cyclohexanone; yields based on the starting PhIO according with Refs. [6,8,10–14,17].
[c] Conditions: MnTMPyP = 2.5×10^{-7} mol, PhIO = 1.0×10^{-5} mol, cyclohexane = 1.5×10^{-3} mol the reactions were carried at room temperature (25 °C), catalytic activities were evaluated as duplicates.
[d] Conditions: MnTMPyP = 3.0×10^{-7} mol, PhIO = 1.5×10^{-5} mol and cyclohexane = 1.5×10^{-3} mol, the reactions were at room temperature (25 °C).
[e] Reactions were conducted in the absence of the MePs in the supports.

In addition, the non-aligned magnetic mesoporous catalyst (Fe_3O_4-NM-MnP) showed higher cyclohexanol and cyclohexanone yields (36% and 9%, respectively, Table 4, entry 6), where the larger pore diameters of the Fe_3O_4-NM-MnP catalyst in relation to aligned mesoporous catalyst (Fe_3O_4-AM-MnP) explain the better results of the catalytic performance. In comparison to similar structures, such as the Fe_3O_4@*n*SiO_2@MCM-41 formerly reported by our group [19], both aligned and non-aligned mesoporous catalysts showed a slightly lower selectivity when a 1:10 catalyst:oxidant molar ratio is applied. However, the present results reveal that the Fe_3O_4-NM-MnP and Fe_3O_4-AM-MnP are able to maintain the selectivity even in the presence of a larger amount of oxidant (1:40 catalyst:oxidant molar ratio, Table 4, entries 4 and 6).

The comparison between the Fe_3O_4-AM-FeP and Fe_3O_4-NM-FeP catalysts with the preparation containing FeP immobilized at surface (Fe_3O_4-SM-FeP showed an improved selectivity (Table 4, entries 11-16). These results are consistent with literature, since FeP is known to be the best biomimetic system [43,44], as observed from our results on alcohol/ketone selectivity achieved in the reactions using the FeP in homogenous catalysis (Table 4, entries 9 and 10). In addition, results in Table 4 also reveal that both for the homogeneous and heterogeneous catalysis, the application of a higher MeP:PhIO ratio (1:40) does not result in significant alterations on the catalyst performance provided by the prepared compounds, thus confirming that larger contents of oxidant do not lead to the loss of catalytic activity. Furthermore, it is clearly observed the increase of the efficiency catalysis when use DCE/ACN as solvent (Table 4, entries 12, 14 and 16).

The materials Fe_3O_4-AM-(MnTMPyP) and Fe_3O_4-NM-(MnTMPyP) containing the cationic (MnTMPyP) porphyrin prepared by a post-synthesis process, were also investigated with regard to cyclohexane oxidation. The results in Table 5 (entries 2-6) evidence higher global yields of cyclohexane oxidation for the Fe_3O_4-AM-(MnTMPyP) and Fe_3O_4-NM-(MnTMPyP) catalysts in comparison to homogeneous catalysis results (Table 5, entry 1).

The prepared compounds display a higher global oxidation performance in comparison to conventional core-shell systems described by Ucoski et al. [17], where cyclohexanol yields of 2% in 1 h of reaction are reported. In the present work, we achieved 13% yield (Fe_3O_4-AM-(MnTMPyP), Table 5, entry 6) in the same catalytic conditions. Regarding long reaction times (24 h), results of cyclohexanol yields here described are also high (26% for Fe_3O_4-AM-(MnTMPyP), Table 5, entry 2) in comparison to other supports containing MnTMPyP described in the literature [45]. Besides, the Fe_3O_4-AM-(MnTMPyP) catalyst showed higher selectivity in 1 h of catalysis (Table 5, entries 3 and 5). The catalytic results with cationic porphyrin are promising because it is less expensive compared to the fluorinated porphyrins, besides displaying an easy *post synthesis* immobilization in the magnetic silica mesoporous supports. Another advantage to be highlighted is the catalytic reactions in DCE (Table 5 entries, 4 and 5), as these results showed that the immobilization of the MnTMPyP minimizes the problems of low solubility of cationic porphyrins in organic solvents [17], thus expanding the possible use of these systems in drug metabolism studies [7]. In addition, in the context of the ecofriendly catalysis, the magnetic core@shell mesoporous material showed can also be used with nonhalogenated solvents in catalysis reactions. In others words, catalysts maintained the selectivity toward cyclohexanol during cyclohexane oxidation (Table 6, entries 1-6) when a toluene:ethanol (1:1) mixture was used as catalysis solvent. These results reinforce the hypothesis that magnetic core@shell mesoporous materials are a better supports for immobilization of the metalloporphyrins than conventional magnetic core@shell materials reported by literature [17].

Finally, control reactions carried out in the absence of MePs (Table 4; entries 12-14; Table 5, entries 17-20; Table 6, entries 7 and 8) do not lead to detectable amounts of oxidation products, so the catalytic activity of the prepared compounds is indeed due to the presence of MePs in the obtained core@shell mesoporous systems. We also analyzed the supernatants of all the heterogeneous catalysis reactions by UV–Vis spectroscopy, where no

Table 6
Cyclohexane oxidation by PhIO catalyzed by FeP and MnP in heterogeneous catalysts with mixture, toluene:ethanol (1:1) as solvents.

Entry	Catalyst	%C_{ol} (±7%)	%C_{one} (±2%)	C_{ol}/C_{one}[b]
1	Fe_3O_4-AM-MnP[c]	8.0 (13)[a]	1.0 (3.0)	8.0 (4.0)
2	Fe_3O_4-NM-MnP[c]	15 (16)	1.0 (6.0)	15 (2.5)
3	Fe_3O_4-NM-FeP[c]	8.0 (12)	1.0 (2.0)	8.0 (6.0)
4	Fe_3O_4-AM-FeP[c]	20 (25)	1.0 (7.0)	20 (3.5)
5	Fe_3O_4-AM-(MnTMPyP)[d]	8.0 (14.0)	1.0 (3.0)	8.0 (4.6)
6	Fe_3O_4-NM-(MnTMPyP)[d]	7.0 (17.0)	1.0 (5.0)	7.0 (3.4)
Catalysis control				
7	Fe_3O_4-AM	–	–	–
8	Fe_3O_4-NM	–	–	–

[a] Catalytic results in parentheses were obtained after 24 h of the reactions. Results outside parentheses were obtained after 1 h of the reactions.
[b] C_{ol} = cyclohexanol and C_{one} = cyclohexanone; yields based on the starting PhIO according with Refs. [6,8,10–14,17].
[c] Conditions: MeP = 2.5×10^{-7} mol, PhIO = 1.0×10^{-5} mol, cyclohexane = 1.5×10^{-3} mol, catalytic tests were performed as duplicate.
[d] Conditions: MnTMPyP = 3.0×10^{-7} mol, PhIO = 1.5×10^{-5} mol and cyclohexane = 1.5×10^{-3} mol, the reactions were at room temperature (25 °C).

characteristic bands of MePs were detected. Therefore, this suggests that these complexes did not leach from the supports during the oxidation tests as also reported by Ucoski et al. [17].

4. Conclusions

The present work demonstrates the successful preparation of magnetic core@shell catalysts with aligned (Fe_3O_4-AM-MeP) and non-aligned (Fe_3O_4-NM-MeP) mesoporous silica layers and their performance in hydrocarbon oxidation. The catalysts showed high epoxidation yields, indicating a combined effect of immobilized porphyrins and inorganic hosts. The obtained compounds are also recyclable materials, since they also display excellent magnetic response and a good redispersibility, which provide an easy catalyst recovery from the reaction medium.

The catalysts with aligned or non-aligned silica mesopores showed excellent selectivity toward the production of cyclohexanol compared with homogeneous catalysts, mainly in the case of manganese porphyrins. These results indicate that ordered or disordered mesoporous do not influence the catalysis selectivity. The key conclusion is that the confinement effect of the MePs immobilization provided by the structural features of the aligned or non-aligned silica mesopores might favor the restriction of the MePs orientation within mesochannels and consequently improve selectivity in the cyclohexane oxidation toward cyclohexanol.

In addition, the selective hydrocarbon hydroxylation and excellent epoxidation performance suggests that the high-valence metal-oxo intermediate ($Fe^{IV}(O)P^{+\cdot}$ or $Mn^{V}(O)P$) must be the main catalytic species involved in this system. Therefore, the mesoporous magnetic catalysts have great potential application in fine chemistry, so in future work will focus on the use of these catalysts in aerobic oxidations.

Acknowledgements

The authors thank the Brazilian agencies CAPES, CNPq, and FAPESP (Proc. 2013/01669-1 and 2014/22930-2, PCdSF, and Proc. 2013/08439-1, FBZ) for financial support and scholarships. The authors are also grateful to Prof. A.P. Ramos (University of São Paulo) for the use of instrumental facilities, to Prof. A.F. Nogueira (State University of Campinas) for N_2 adsorption measurements, and to Mr. D.D. Coimbrão (LCE-DEMa-Federal University of São Carlos) for TEM images.

Appendix A. Supplementary material

Supplementary data associated with this article can be found, in the online version, at http://dx.doi.org/10.1016/j.jcis.2016.01.059.

References

[1] B. Meunier, S.P. de Visser, S.P.S. Shaik, Chem. Rev. 104 (2004) 3947–3980.
[2] P.R.O. de Montellano, Chem. Rev. 110 (2010) 932–948.
[3] H.C. Sacco, Y. Iamamoto, J.R.L. Smith, J. Chem. Soc. Perkin Trans. 2 (2001) 181–190.
[4] D. Mansuy, C. R. Chim. 10 (2007) 392–413.
[5] D. Dolphin, T.G. Traylor, L.Y. Xie, Acc. Chem. Res. 30 (1997) 251–259.
[6] J.T. Groves, T.E. Nemo, J. Am. Chem. Soc. 105 (1983) 6245.
[7] M.M.Q. Simões, C.M.B. Neves, S.M.G. Pires, M.G.P.M.S. Neves, J.A.S. Cavaleiro, Pure Appl. Chem. 85 (2013) 1671–1681.
[8] B.R.S. Lemos, D.C. Da-Silva, D.Z. Mussi, L. das Santos, M.M. Silva, M.E.M.D. de Carvalho, J.S. Rebouças, Y.M. Idemori, Appl. Catal. A 400 (2011) 111–116.
[9] J.I.T. Costa, A.C. Tomé, M.G.P.M.S. Neves, J.A.S. Cavaleiro, J. Porphyrins Phthalocyanines 15 (2011) 1116–1133.
[10] V.S. da Silva, L.I. Teixeira, E. do Nascimento, Y.M. Idemori, G. DeFreitas-Silva, Appl. Catal. A 469 (2014) 124–131.
[11] J.R. Lindsay-Smith, Y. Iamamoto, F.S. Vinhado, J. Mol. Catal. A: Chem. 252 (2006) 23–30.
[12] G.S. Machado, O.J. Lima, K.J. Ciuffi, F. Wypych, S. Nakagaki, Catal. Sci. Technol. 3 (2013) 1094–1096.
[13] L.B. Bolzon, H.R. Airoldi, F.B. Zanardi, J.G. Granado, Y. Iamamoto, Microporous Mesoporous Mater. 168 (2013) 37–45.
[14] J. Połtowicz, E.M. Serwicka, E. Bastardo-Gonzalez, W. Jones, R. Mokaya, Appl. Catal. A 218 (2001) 211–217.
[15] B. Yan, Y.-Y. Li, X.-F. Qiao, Microporous Mesoporous Mater. 158 (2012) 129–136.
[16] M.J.F. Calvete, M. Silva, M.M. Pereira, H.D. Burrows, RSC Adv. 3 (2013) 22774–22789.
[17] G.M. Ucoski, F.S. Nunes, G.de. Freitas-Silva, Y.M. Idemori, S. Nakagaki, Appl. Catal. A 459 (2013) 121–130.
[18] C.M.B. Carvalho, E. Alves, L. Costa, J.P.C. Tomé, M.A.F. Faustino, M.G.P.M.S. Neves, A.C. Tomé, J.A.S. Cavaleiro, A. Almeida, A. Cunha, Z. Lin, J. Rocha, ACS Nano 12 (2010) 7133–7140.
[19] F.B. Zanardi, I.A. Barbosa, P.C. de Sousa Filho, L.D. Zanatta, D.L. da Silva, O.A. Serra, Y. Iamamoto, Microporous Mesoporous Mater. 219 (2016) 161–171.
[20] Y. Deng, Y. Cai, Z. Sun, D. Zhao, Chem. Phys. Lett. 510 (2011) 1–13.
[21] J. Liu, S.Z. Qiao, Q.H. Hu, G.Q.M. Lu, Small 7 (2011) 425–443.
[22] Y. Deng, D. Qi, C. Deng, X. Zhang, D. Zhao, J. Am. Chem. Soc. 130 (2008) 28–29.
[23] H. Liu, S. Ji, H. Yang, H. Zang, M. Tang, Ultrason. Sonochem. 21 (2014) 505–512.
[24] G. Huang, L.-Q. Mo, J.-L. Cai, X. Cao, Y. Peng, Y.-A. Guo, S.-J. Wei, Appl. Catal. B: Environ. 162 (2015). 364-37.
[25] C.-C. Guo, X.-Q. Liu, Q. Liu, Y. Liu, M.-F. Chu, W.-Y. Lin, J. Porphyrins Phthalocyanines 13 (2009) 1250–1254.
[26] O. Herrmann, S.H. Mehdi, A. Corsini, Can. J. Chem. 56 (1978) 1084–1087.
[27] J.G. Sharefkin, H. Saltzman, Org. Synth. 43 (1963) 62.
[28] H. Zhang, X. Zhong, J.-J. Xu, H.-Y. Chen, Langmuir 24 (2008) 13748–13752.
[29] G.S. Nunes, I. Mayer, H.E. Toma, K. Araki, J. Catal. 236 (2005) 55–61.
[30] H. Deng, X.L. Li, Q. Peng, X. Wang, J.P. Chen, Y.D. Li, Angew. Chem. Int. Ed. 44 (2005) 2782–2785.
[31] J.-L. Cao, Z.-L. Yan, Y. Wang, G. Sun, X.-D. Wang, H. Bala, Z.-Y. Zang, Mater. Lett. 106 (2013) 322–325.
[32] P. Chagas, H.S. Oliveira, R. Mambirini, M.L. Hyaric, M.V. Almeida, L.C.A. Oliveira, Appl. Catal. A 454 (2013) 88–92.
[33] M.P.S. Almeida, K.L. Caiado, P.P.C. Sartoratto, D.O. Cintra e Silva, A.R. Pereira, P. C.J. Morais, J. Alloys Compd. 500 (2010) 149–152.
[34] P.C. Morais, S.W. Silva, M.A.G. Soler, N. Buske, Biomol. Eng. 17 (2001) 41–49.
[35] Z.U. Rahman, Y.-L. Dong, L. Su, Y.-H. Ma, H.-J. Zhang, X.-G. Chen, Chem. Eng. J. 222 (2013) 382–390.
[36] Z. Wua, H. Xiang, T. Kima, M.-S. Chun, K. Lee, J. Colloid Interface Sci. 304 (2006) 399–402.
[37] K.S.W. Sing, D.H. Everett, R.A.W. Haul, L. Moscou, R.A. Pierotti, J. Rouquerol, T. Siemineieweka, Pure Appl. Chem. 57 (1985) 603–619.
[38] P.P. Yang, Z.W. Quan, Z.Y. Hou, C.X. Li, X.J. Kang, Z.Y. Cheng, J. Lin, Biomaterials 30 (2009) 4786–4795.
[39] J.R. Lindsay-Smith, in: R.A. Sheldon (Ed.), Metalloporphyrins in catalytic oxidation, Marcel Dekker, New York, 1994, pp. 325–361.
[40] J.S. dos Santos, A.L. Faria, P.M.S. Amorin, F.M.L. Luna, K.L. Caiado, D.O.C. Silva, P. P.C. Sartoratto, M.D. Assis, J. Braz. Chem. Soc. 23 (2012) 1–10.
[41] J.T. Groves, J. Inorg. Biochem. 100 (2006) 434–447.
[42] J.N. Junior Sousa, B.A. Rocha, M.D. de Assis, A.P.F. Peti, L.A.B. Moraes, Y. Iamamoto, P.J. Gates, A.R.M. de Oliveira, N.P. Lopes, Braz. J. Pharmacog. 23 (2013) 621–629.
[43] M.A. Schiavon, Y. Iamamoto, O.R. Nascimento, M.D. Assis, J. Mol. Catal. A 174 (2001) 213–222.
[44] Y. Iamamoto, M.D. Assis, K.J. Ciuffi, C.M.C. Prado, B.Z. Prellwitz, M. Moraes, R. Nascimento, H.C. Sacco, J. Mol. Catal. A 116 (1997) 365–374.
[45] L.P.B. Lôvo, F.C. Skrobot, G.C. Azzellini, Y. Iamamoto, I.L.V. Rosa, Mod. Res. Catal. 2 (2013) 47–55.